Robust Meteorological Drought Prediction Using Antecedent SST Fluctuations and Machine Learning

Article *in* Water Resources Research · August 2021

DOI: 10.1029/2020WR029413

CITATIONS
8

READS
595

7 authors, including:

Zhaoli Wang
South China University of Technology
1,015 PUBLICATIONS **9,624** CITATIONS
SEE PROFILE

Xushu Wu
South China University of Technology
338 PUBLICATIONS **3,088** CITATIONS
SEE PROFILE

Chong-Yu Xu
University of Oslo
533 PUBLICATIONS **22,061** CITATIONS
SEE PROFILE

Shenglian Guo
Wuhan University
383 PUBLICATIONS **9,055** CITATIONS
SEE PROFILE

Water Resources Research

RESEARCH ARTICLE
10.1029/2020WR029413

Robust Meteorological Drought Prediction Using Antecedent SST Fluctuations and Machine Learning

Jun Li[1,2], Zhaoli Wang[1,2], Xushu Wu[1,2], Chong-Yu Xu[3], Shenglian Guo[4], Xiaohong Chen[5], and Zhenxing Zhang[6]

[1]School of Civil Engineering and Transportation, State Key Laboratory of Subtropical Building Science, South China University of Technology, Guangzhou, China, [2]Guangdong Engineering Technology Research Center of Safety and Greenization for Water Conservancy Project, Guangzhou, China, [3]Department of Geosciences, University of Oslo, Oslo, Norway, [4]State Key Laboratory of Water Resources and Hydropower Engineering Science, Wuhan University, Wuhan, China, [5]Center for Water Resource and Environment, Sun Yat-Sen University, Guangzhou, China, [6]Illinois State Water Survey, Prairie Research Institute, University of Illinois, Champaign, IL, USA

Key Points:

- Antecedent sea surface temperature fluctuations are introduced as predictors for meteorological drought prediction
- Extreme learning machine predicts droughts more effectively than support vector regression and random forest
- The new approach allows for ensemble, probability, and deterministic drought predictions

Supporting Information:

Supporting Information may be found in the online version of this article.

Correspondence to:

X. Wu,
xshwu@scut.edu.cn

Citation:

Li, J., Wang, Z., Wu, X., Xu, C.-Y., Guo, S., Chen, X., & Zhang, Z. (2021). Robust meteorological drought prediction using antecedent SST fluctuations and machine learning. *Water Resources Research*, *57*, e2020WR029413. https://doi.org/10.1029/2020WR029413

Received 12 DEC 2020
Accepted 11 JUL 2021

Abstract While reliable drought prediction is fundamental for drought mitigation and water resources management, it is still a challenge to develop robust drought prediction models due to complex local hydro-climatic conditions and various predictors. Sea surface temperature (SST) is considered as the fundamental predictor to develop drought prediction models. However, traditional models usually extract SST signals from one or several specific sea zones within a given time span, which limits full use of SST signals for drought prediction. Here, we introduce a new meteorological drought prediction approach by using the antecedent SST fluctuation pattern (ASFP) and machine learning techniques (e.g., support vector regression (SVR), random forest (RF), and extreme learning machine (ELM)). Three models (i.e., ASFP-SVR, ASFP-ELM, and ASFP-RF) are developed for ensemble, probability, and deterministic drought predictions. The Colorado, Danube, Orange, and Pearl River basins with frequent droughts over different continents are selected, as the cases, where standardized precipitation evapotranspiration index (SPEI) are predicted at the 1° × 1° resolution with 1- and 3-month lead times. Results show that the ASFP-ELM model can effectively predict space-time evolutions of drought events with satisfactory skills, outperforming the ASFP-SVR and ASFP-RF models. Our study has potential to provide a reliable tool for drought prediction, which further supports the development of drought early warning systems.

1. Introduction

Drought is one of the severe natural hazards that imposes destructive effects on a wide range of sectors including economy and ecosystems (Li et al., 2021; Williams et al., 2020). Drought control and disaster mitigation require timely and reliable drought predictions that provide essential information to develop and implement feasible drought mitigation measures (Li, Wang, Wu, Xu, et al., 2020; Ma et al., 2019; Sutanto et al., 2020). In general, drought prediction methods include dynamical and statistical predictions. Although dynamical models provide useful information for drought situations based on the short-term climatic forecasting, it is usually difficult to implement in applications at local agencies due to complex procedures, especially for undeveloped regions (Chen & Georgakakos, 2014). In addition, it contains uncertainty and limited skill with respect to long lead times (Liu et al., 2018). Alternatively, statistical models that utilize macro-scale interconnections between oceanic and atmospheric variables are relatively simple but perform as well as or even better than the dynamical ones (Deo et al., 2017). Therefore, some scientists and managers still rely on statistical models for practical applications (Chen & Georgakakos, 2014).

To date, much effort has made to develop reliable and effective statistical drought prediction models by developing new or improved methods and selecting most related predictors. Both linear and nonlinear models have been widely used to construct the interconnections between predictor and predictand (Agha-Kouchak, 2014). For example, autoregressive integrated moving average models have been the most widely used stochastic models for hydrological drought prediction (Tian et al., 2016). Nevertheless, the relationships between predictor and predictand are somewhat nonlinear (Mishra & Singh, 2012). Machine learning algorithms, such as Support Vector Regression (SVR), Random forest (RF), and extreme learning machine (ELM), are thus introduced to address the limitation of linear models (Belayneh & Adamowski, 2012;

Belayneh et al., 2014; Feng et al., 2020). These three models have been extensively applied in various fields, such as floods and precipitation prediction (Ali et al., 2020; Lee et al., 2017; Sadler et al., 2018).

SVR is a machine learning method, popular in hydrological prediction (Khan & Coulibaly, 2006; Rasouli et al., 2012). Belayneh and Adamowski (2012) utilized SVR to predict the standardized precipitation index (SPI) in the Awash River basin. To improve prediction accuracy, the wavelet transforms were applied to the pre-processing of SVR, forming the wavelet-SVR model (Belayneh et al., 2014). Zeng et al. (2011) found that SVR has better prediction skill in predicting winter extreme precipitation than the multiple linear regression and Bayesian neural network models. RF is generally used for drought prediction over different drought prone regions around the world (Dikshit et al., 2020; Loken et al., 2019). Based on RF, drought prediction models were developed for South Korea (Rhee & Im, 2017). For East Asia, Park et al. (2018) constructed a short-term meteorological drought prediction model by employing RF and using the Madden-Julian oscillation index as the predictor. Extreme learning machine (ELM) is another widely used method in hydroclimate prediction (Lima et al., 2016; Niu et al., 2020). For example, Li and Cheng (2014) conducted 1-month ahead monthly discharge prediction for two reservoirs located in southwestern China, and demonstrated that the ELM-based model performed slightly better than SVM for peak discharge estimation. Lima et al. (2015) also demonstrated that ELM outperformed other commonly used models such as the multiple linear regression, SVR, RF, and artificial neural networks in terms of the computational efficiency.

For predictor screening, the factors that reflect large-scale atmospheric and oceanic conditions are usually considered for hydroclimate prediction, among which sea surface temperature (SST) is one of the strongest signals (Manzano et al., 2019). As indicated by Dai (2011) and Schubert et al. (2016), there is close relationship between SST and large-scale atmospheric circulation and SST plays a significant role in driving hydro-climatic variability. As such, SST is commonly used for hydro-climatic predictions (Hao et al., 2018). Using SST, together with Pacific-North American atmospheric teleconnection and Pacific Decadal Oscillation, linear- and nonlinear-based models were developed for prediction of the April-August streamflow in the Columbia River, Canada (Hsieh et al., 2003). Diro et al. (2011a) developed a seasonal precipitation prediction system over Ethiopia based on the linkage between global SST and precipitation anomalies. Funk et al. (2014) discovered that the eastern African boreal spring precipitation variability is related to SST fluctuations, and determined SST indices to predict spring precipitation in eastern African. While in China, a prediction model for large and regional scale droughts was developed based on drought-related SST (Liu et al., 2018).

Meteorological drought prediction is important for predicting other types of droughts, since water deficit may propagate to the relevant component of the hydrological cycle (Hao & Singh, 2016). Although the aforementioned studies employing SST as the drought predictor are useful and encouraging, developing a general, accurate meteorological drought prediction model still remains a challenge (Madadgar et al., 2016). On one hand, most of drought prediction models utilize SST signals over one or some specific sea zones (Belayneh et al., 2014; Feng et al., 2020; Madadgar et al., 2016). For example, the nino3.4, one of the indicator of El Niño-Southern Oscillation (ENSO), is referred to as the average SST anomaly in the region bounded by 5°N–5°S and 170°–120°W. Consequently, the potential useful information of SST over other sea zones are neglected, limiting the model inputs and in turn hampering the improvement of model accuracy (Chen & Georgakakos, 2014). Moreover, there is still a lack of consideration of the temporal fluctuation of SST. Many studies extract SST signals in such a way that SST is averaged over a time span (e.g., wintertime SST and monthly SST), or SST over different time periods is used separately (e.g., September SST and October SST are regarded as two separate predictors). In fact, the temporal SST fluctuation is indicative of hydro-climatic variables variations. It is possible that through using SST fluctuation the accuracy of drought prediction model improves. On the other hand, under the backdrop of climate change, meteorological droughts in future probably show larger uncertainties than the past, making deterministic drought prediction models less informative for drought control and disaster mitigation (Xu et al., 2018). In this regard, ensemble or probability prediction is beneficial and essential, since it provides more information than deterministic prediction for decision or policy makers to manage meteorological droughts.

In terms of drought characterization, precipitation-based drought indices such as SPI are often utilized for drought monitoring and prediction. However, the index that only involves precipitation neglects the other climate factors (e.g., temperature and potential evapotranspiration), and it assumes the stationarity

of other variables (Vicente-Serrano et al., 2010). The SPI-based drought prediction may deviate from the actual dry situations (Rhee & Im, 2017). Drought indices like standardized precipitation evapotranspiration index (SPEI) are more preferable, especially for applications involving drought prediction in complicated and changing climate scenarios (Vicente-Serrano et al., 2010).

This then is the focus of our study, where we introduced a new drought prediction approach, capable of making ensemble, probability and deterministic prediction of meteorological droughts across different river basins around the world with relatively high accuracy. The antecedent SST fluctuation pattern (ASFP) is defined and served as the predictor. Three machine learning algorithms, that is, SVR, RF, and ELM are employed to develop models to predict SPEI with 1- and 3-month lead times. To demonstrate our approach, four river basins including the Colorado, Danube, Orange, and Pearl River basins with different climates and frequent droughts are chosen as the cases. We hope that our approach help provide timely and reliable outlooks of droughts to mitigate adverse drought impacts and improve water resource management.

2. Methodology

2.1. Rationale of Drought Prediction Approach

The new drought prediction approach includes three key steps. The first step is to pre-process predictor and predictand, and the second step is to define predictor, followed by the last step in which machine learning is employed to form ensemble, probability, and deterministic drought prediction models. The flowchart of the drought prediction approach is depicted in Figure 1.

2.1.1. Predictor/Predictand Decomposition

The linear and nonlinear methods usually have limited ability to predict non-stationary series; they often fail to handle non-stationary data without input data pre-processing (Belayneh et al., 2014). Therefore, handling non-stationary data requires pre-processing. One traditional data pre-processing way is to use wavelet transforms (Belayneh et al., 2014). Another widely used data pre-processing method is the seasonal-trend decomposition procedure based on loess (STL-decomposition), a simple and robust method for decomposing time series (Sun et al., 2019). The main advantage of this method is that it has strong resilience to outliers, resulting in robust component sub-series. Moreover, based on numerical methods, it can be utilized to a large number of series without the restriction of the properties of each time series (Verbesselt et al., 2010).

In this study, we employ STL-decomposition to decompose SST and SPEI into additive components of variation (trend, seasonality, and residual) instead of the wavelet transforms. Wavelet transforms produce the number of decomposition levels that must be carefully selected (Belayneh et al., 2014). Given that the models in our study would predict droughts at the grid scale, the decomposition levels could differ from one grid to another with the wavelet transforms applied, which leads to much difficulty in selecting decomposition levels. In comparison, the decomposed component from STL-decomposition is more stable. For each decomposition component, a prediction model is established, and the prediction of each sub-component is added together to form the final prediction.

2.1.2. Antecedent SST Fluctuation Patterns

SST predictors based on SST fluctuations between two periods or regions can infer seasonal fluctuations in climate system (Diro et al., 2011a, 2011b; Frankignoul, 1985). It is possible that using the superposition/difference of SSTs between different periods or regions has the potential to improve prediction model accuracy. While the lead time for long-range hydro-climatic prediction can range from month to year (Gobena et al., 2013), the prediction accuracy would decrease and uncertainty enlarge along with increased lead times, probably due to climate change (Chen & Georgakakos, 2014). To reduce prediction uncertainty caused by long lead times, it is better to screen the most recent predictor signals. Meanwhile, the 1–3-month lead time predictions are more accurate than those with longer lead times (Rhee & Im, 2017). We thus select 1–3 months antecedent SST as the predictors.

For the 1-month lead time prediction, the antecedent SST fluctuation pattern is defined by using 1- to 3-month antecedent SST. Define K_1, K_2, and K_3 as the 1–3-months antecedent SST, respectively, and ASFPs are the combination of the 1–3-month antecedent SST superposition or difference.

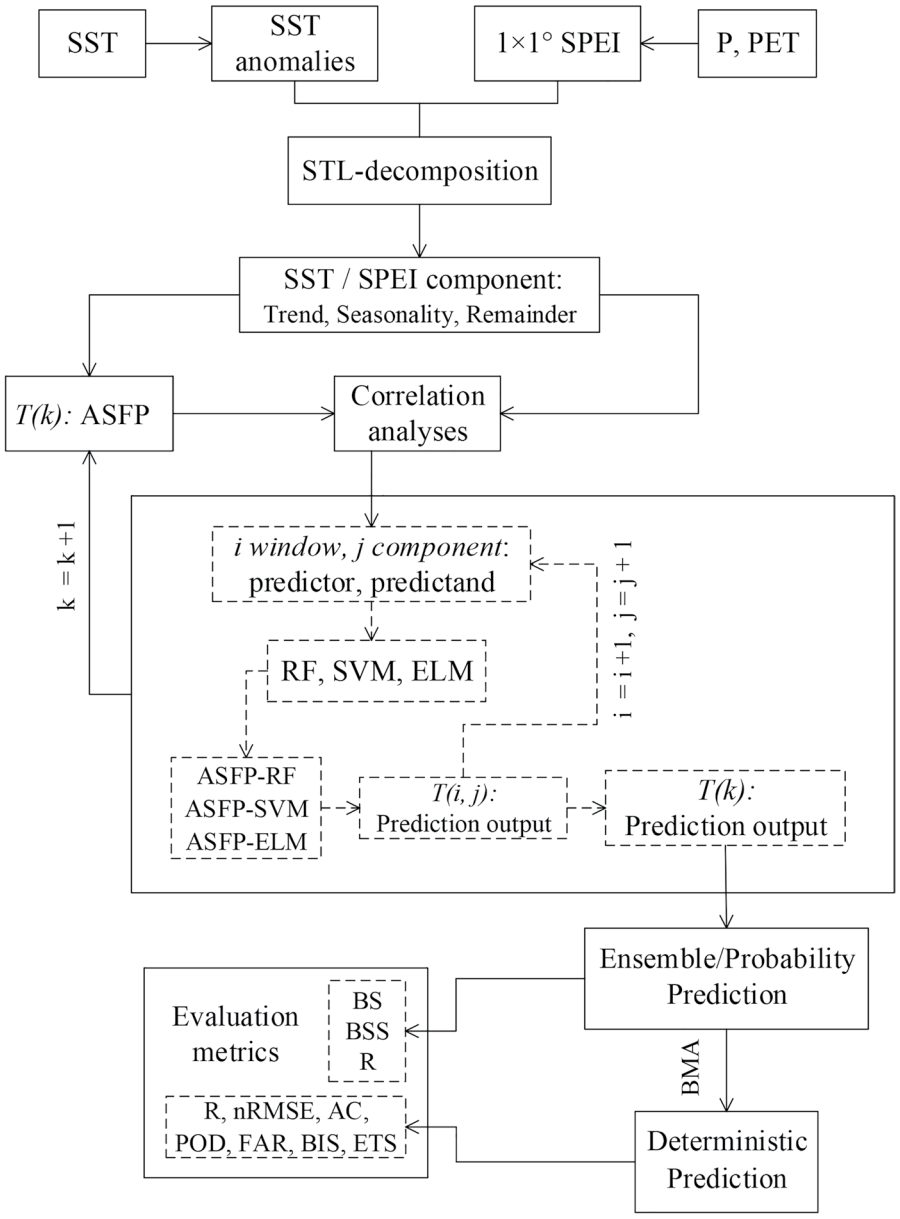

Figure 1. Flow diagram of the meteorological drought prediction approach based on ASFP and machine learning.

1. Type I: include 1 month antecedent SST signals:

$$\mathrm{ASFP1} = K_1. \tag{1}$$

2. Type II: include 2 months antecedent SST signals:

$$\begin{aligned} \mathrm{ASFP2} &= K_1 + K_2, \quad \mathrm{ASFP3} = K_1 - K_2, \\ \mathrm{ASFP4} &= K_1 - K_3, \quad \mathrm{ASFP5} = K_1 + K_3, \end{aligned} \tag{2}$$

3. Type III: include 3 months antecedent SST signals:

$$\begin{aligned} \mathrm{ASFP6} &= K_1 + K_2 + K_3, \quad \mathrm{ASFP7} = K_1 - K_2 - K_3, \\ \mathrm{ASFP8} &= K_1 + K_2 - K_3, \quad \mathrm{ASFP9} = K_1 - K_2 + K_3, \end{aligned} \tag{3}$$

The nine ASFPs are for the 1-month lead prediction. Alternatively, the 3–6 months antecedent SSTs are for the establishment of ASFPs for the 3-months lead prediction.

2.1.3. Predictor Screening

It is essential to identify suitable predictors that can explain large variances of the predictand in certain periods before the setup of a prediction model (Liu et al., 2018). One way to screen predictors is the linear correlation method. Though it could miss the nonlinear relationship between predictor and predictand, it is still the most commonly used tool for diagnosing and selecting potential predictors (Hao et al., 2018). Previous literatures also indicate that models using correlation analysis to select predictors could show predictive skills for different regions (Feng et al., 2020; Hsieh et al., 2003; Rasouli et al., 2012). In this study, the moving time window method is employed; for a moving window, the correlation between a decomposition component (i.e., trend, seasonality and residual) of ASFP (predictor) and that of SPEI (predictand) is examined (Figure S1). The 0.05 significant level is used to identify significant oceanic grids.

2.1.4. Machine Learning Algorithms

When a predictor is screened through correlation analysis, it is not necessarily linearly correlated with predictand. Machine learning algorithm can explore the potential nonlinear connection and has the potential to improve prediction accuracy (Belayneh et al., 2014). Of the various machine learning algorithms, RF, SVR, and ELM are widely employed for hydro-climatic predictions (Dikshit et al., 2020; Niu et al., 2020; Zeng et al., 2011). The three algorithms show many advantages over others, such as high prediction ability and acceptable tolerance to outliers and noise (Huang et al., 2006). As such, these three models have been widely applied to many fields including, but not limited to, hydro-climatic researches (Ali et al., 2020; Lee et al., 2017; Sadler et al., 2018). Therefore, we use the three machine learning algorithms to build drought prediction models.

RF is a combination classification or regression method based on the statistical learning theory (Breiman, 2001). In a RF, multiple samples are drawn using the resampling bootstrap method, and regression trees are built corresponding to each bootstrap sample. SVR is also a regression prediction tool that uses machine learning theory to maximize predictive accuracy while automatically avoiding over-fitting (Chang & Lin, 2011). ELM is a simple and efficient single-hidden layer feedforward network (Huang et al., 2006). Its key idea is to randomly generate the weights between the input layer and the hidden layer, and analytically calculate the output weights by using Moore-Penrose generalized inverse.

2.1.5. Prediction Model Formulation

For the decomposition components (trend, seasonality, and residual) of ASFP and SPEI, the relationship between them is established using the three machine learning algorithms, forming drought prediction models (hereafter ASFP-RF, ASFP-SVR, and ASFP-ELM). The calibration and validation of the models are conducted with the moving time window method (Figure S1). Since there are nine ASFPs, for a decomposition component of SPEI, nine prediction outputs are obtained and the final prediction of SPEI is produced by adding each decomposition component of SPEI. Nine SPEIs would be obtained composing ensemble and probability prediction, which can also be used for deterministic prediction. To obtain a deterministic prediction, merging multiple models is an effective way to alleviate the uncertainties from a single result and to obtain a robust deterministic prediction (Kim et al., 2017). The Bayesian model averaging method is adopted for ensemble averaging (Wang et al., 2017).

2.2. Model Performance Evaluation

The Brier score (BS) and Brier skill score (BSS) are used to estimate ensemble and probability prediction accuracy. The BS is negatively oriented ($0 \leq BS \leq 1$), with perfect prediction $BS = 0$. A positive BSS indicates a better prediction, while a negative value indicates a worse prediction than the reference system that refers to the threshold of SPEI that identifies drought events (Muluye, 2011). A threshold of -0.5 for SPEI is used which is also widely used elsewhere for identification of drought events (Hateren et al., 2019). The correlation coefficient (r) is for the evaluation of probability and deterministic prediction performance. The normalized Root Mean Square Error (nRMSE) and a contingency table approach (recommended by the World Weather Research Program, https://community.wmo.int/activity-areas/wwrp) are employed to assess deterministic prediction (Feng et al., 2020). If it is lower than 10.0%, the performance of the model is considered excellent; higher than 10.0% but lower than 20.0% indicates good performance; higher than 20.0% but

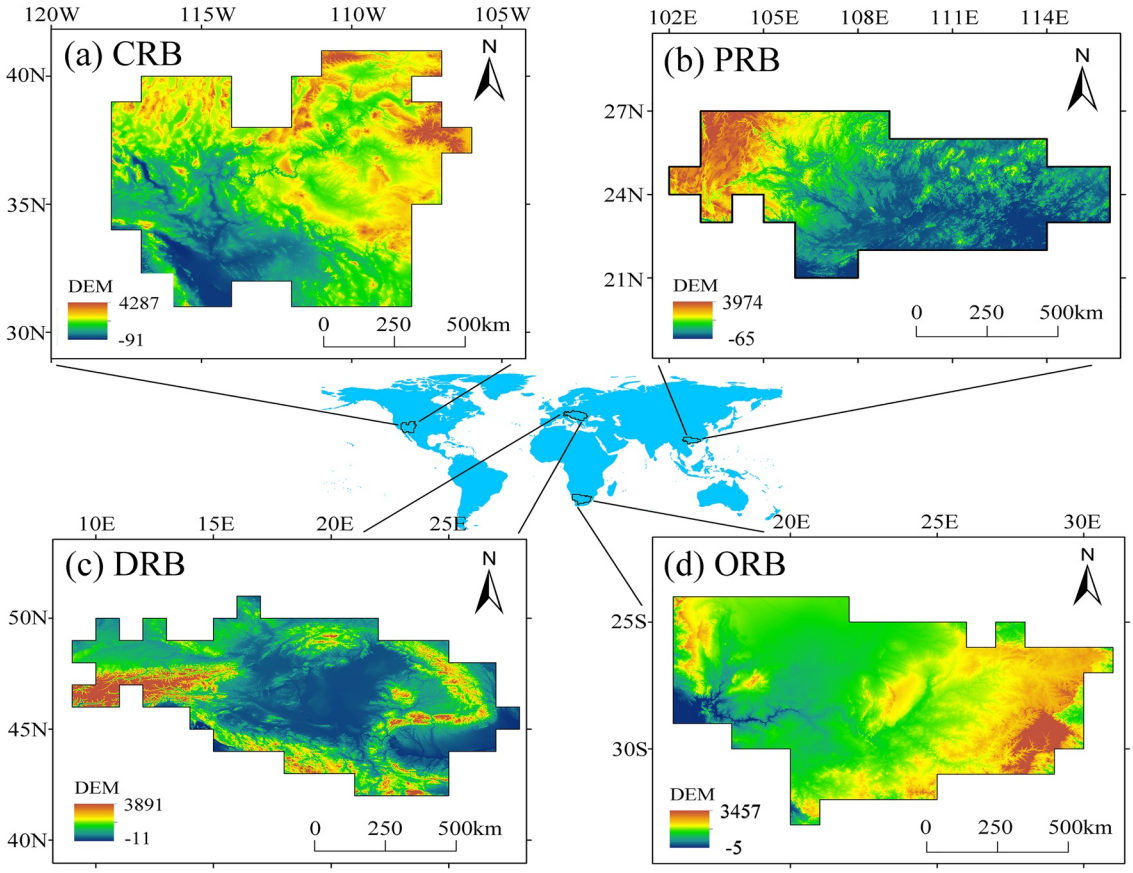

Figure 2. Locations of four river basins used in this study. (a) Colorado River Basin (CRB) in North America, (b) Pearl River Basin (PRB) in Asia, (c) Danube River Basin (DRB) in Europe, and (d) Orange River Basin (ORB) in Africa.

lower than 30.0% suggests fair prediction; higher than 30.0% implies poor prediction (Feng et al., 2020). There are four possibilities, including hit, miss, false alarm and correct negative. At a given lead time, a hit is calculated when both observation and prediction indicate a drought. It is a miss if the observation shows drought while the prediction does not. A false alarm is identified when the prediction indicates a drought but the observation does not. It is a correct negative if no drought occurs in both observation and prediction. From the contingency table, the accuracy (AC), bias score (BIS), probability detection (POD), false alarm ratio (FAR), and equitable threat score (ETS) are derived (Mo & Lettenmaier, 2020).

3. Case Study and Data

3.1. Case Regions

Four river basins are chosen from different continents (respectively located in East Asia, North America, Europe, and Southern Africa, Figure 2) to demonstrate the performance of the presented approach. The first river basin named Pearl River basin (PRB), is the third largest drainage basin in China, with an approximate area of 454,000 km^2. Though it is characterized by the humid climate, it has suffered considerably from frequent and severe meteorological droughts (Li, Wang, Wu, Chen, et al., 2020). The Colorado River basin (CRB) is located within the intermountain region of the western United States. In recent decade, CRB underwent several largest droughts observed in the historical record (He et al., 2017). The third case is the Danube River basin (DRB) in Europe, covering a total area of about 800,000 km^2. The fourth basin is the Orange River basin (ORB) located in Southern Africa, which has an area of about 900,000 km^2. The climates over these four basins are different, varying from humid to arid climates; correspondingly, the drought conditions in these basins are different. Selecting these basins as case regions helps underscore the generality

of the proposed approach. Moreover, these basins suffer from frequent droughts in recent decades that can provide enough drought events for the validation of the approach (Baudoin et al., 2017; He et al., 2017; Masih et al., 2014).

3.2. Data Sources

Monthly 0.5 × 0.5° precipitation and potential evapotranspiration (PET) data sets from the Climatic Research Unit (CRU TS v. 4.03) of the University of East Anglia (Harris et al., 2014) are used to calculate the SPEI in these four basins during 1901–2018. The 3-months SPEI are used as it is considered more stable than 1-month SPEI and more sensitive to the drought processes than those with longer time scales (Zhao et al., 2017). The CRU has strictly validated and controlled the quality of the data, and the Penman-Monteith method is utilized to compute PET. It is a widely used climate data source around the world which is updated in time and reliable for drought application (Beguería et al., 2014). Considering that if the spatial resolution of the prediction models are set too fine, there would be a number of grids resulting in exceptional computation burden, while too coarse could hinder precise prediction. Finally, the prediction models are developed at the spatial resolution of 1° × 1° and SPEI are thus resampled to such resolution by the bilinear interpolation. The National Oceanic and Atmospheric Administration COBE-SST data set with 1° × 1° resolution from 1901 to 2018 is used for SST anomaly analysis (Ishii et al., 2005). Like CRU data, COBE-SST data are open accessed and updated in time, which supports the development of SST-based monthly or seasonal drought prediction models.

3.3. Model Setup and Parameter Specification

In the case study, we select some oceanic regions where predictors (ASFP) are screened from for four basins (Figure S2), given that the computational cost might be huge if global SST is involved. The time moving window is set to 30-year length resulting in 30 calibration periods (i.e., 1901–1988, 1902–1989, ..., 1930–2017) and 30 validation outputs (i.e., 1989, 1990, ..., 2018). In addition, the e-SVR is used in the study, along with "elmNNRcpp," "e1071," and "randomForest" packages in the *R* software, to drive ELM, SVR and RF models.

The impact of hidden neurons in ELM (or regression trees in RF) on model accuracy are assessed. Simulation and prediction results during calibration and validation are obtained according to different hidden neurons (or regression trees). During calibration, for each ASFP and sub-decomposition model, the *r* and RMSE values between observation and simulation are calculated at each grid in each widow; while during validation, the BS and BSS values for ensemble prediction and *r* values for deterministic prediction are calculated. The parameter specification and the corresponding results are shown in Figures S3–S6. The hidden neurons for ASFP-ELM model is set to 300, and the regression trees for ASFP-RF model is set to 500. As for ASFP-SVR model, the "tune" function in the "e1071" R package is used to select the optimal parameter.

4. Results

4.1. Ensemble and Probability Predictions

Using the ensemble prediction from 1989 to 2018, BS and BSS are calculated to evaluate ensemble prediction (Figure 3). For 1-month lead time prediction, the ASFP-ELM model overall shows lower BS values than that driven by ASFP-RF and ASFP-SVR models in these four basins. BS values of the ASFP-ELM model are mostly less than 0.15 across most of the study areas in four basins (Figure 3a). However, they mostly range from 0.2 to 0.3 for the ASFP-RF and ASFP-SVR models in PRB, DRB, and CRB; high BS values were found in ORB, with a range of 0.3–0.4. BSS values are mostly larger than 0.4 for most areas of the four basins according to the ASFP-ELM model (Figure 3b). Nevertheless, the BSS values are less than 0.2 for the ASFP-RF and ASFP-SVR models across the most areas of the PRB, DRB, and CRB, and are lower than 0 in ORB. The BS and BSS values of the 3-months lead time prediction share similar spatial pattern with those of the 1-month lead prediction (Figures 3c and 3d). Low BS values are found in most parts of the four basins for the ASFP-ELM model, ranging from 0 to 0.15 (Figure 3c). In contrast, the ASFP-RF and ASFP-SVR models show larger BS values, ranging from 0.2 to 0.3. Figure 3d indicates that most areas of the four basins present

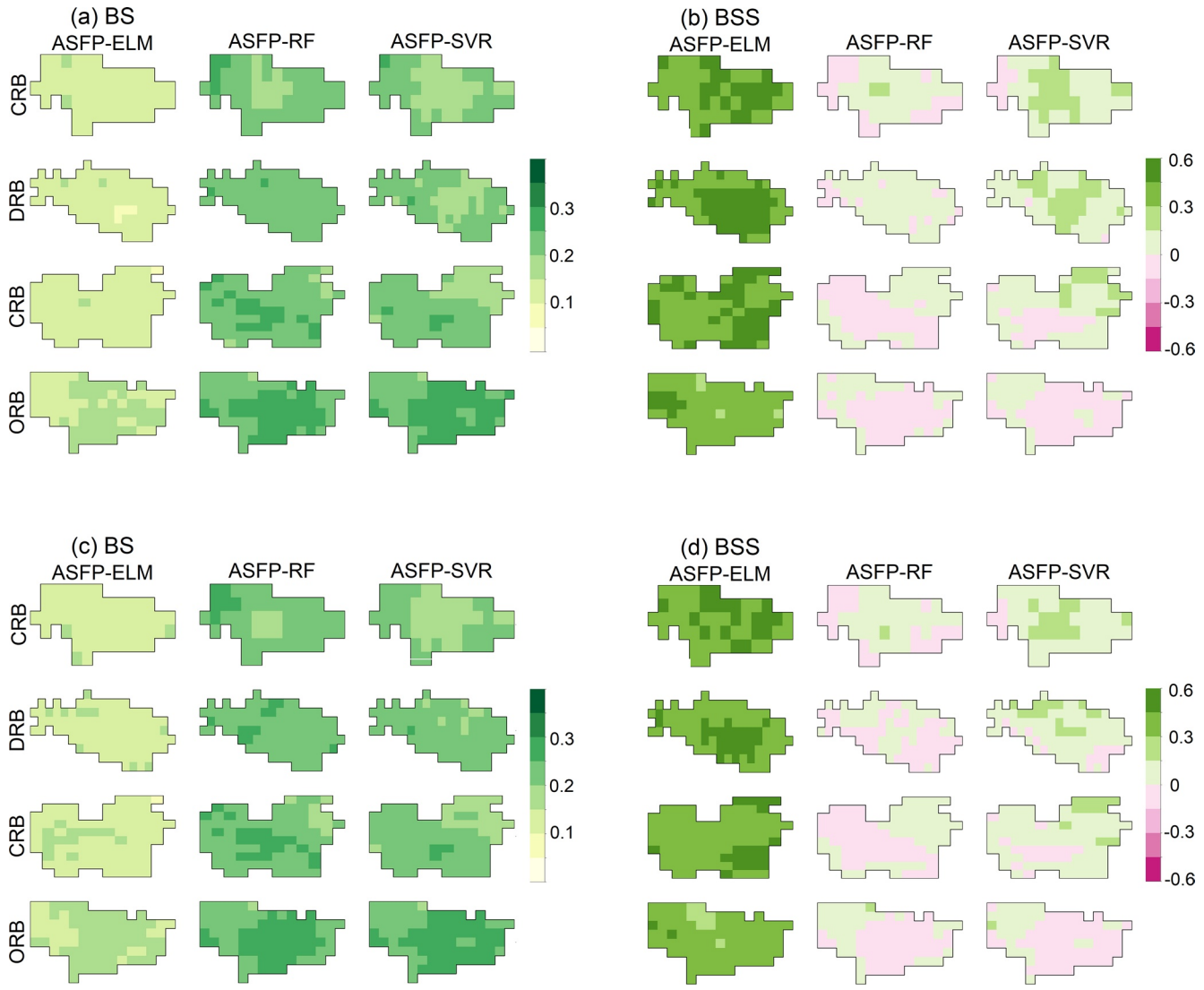

Figure 3. The BS and BSS metrics for ensemble prediction of the three models in four river basins. (a and b) 1-month lead prediction; (c and d) 3-months lead prediction.

satisfied BSS values based on the ASFP-ELM model, with a range of 0.3–0.4. However, BSS values of the ASFP-RF and ASFP-SVR models in most parts of the study areas are less than 0.2.

The BS and BSS values of probability prediction are similar to those of ensemble prediction (Figure 4). The ASFP-ELM model in four basins present lower BS values, with a range of 0–0.15. In contrast, the ASFP-RF and ASFP-SVR models display relatively larger BS values ranging from 0.2 to 0.3. Moreover, most areas of the study regions show satisfactory BSS values for the ASFP-ELM model, with a range of 0.3–0.4. However, BSS values of the ASFP-RF and ASFP-SVR models in most parts of the study areas are less than 0.2. In addition, r values of ASFP-ELM model are lower than those of ASFP-RF and ASFP-SVR in the study regions. Specifically, r values of the ASFP-ELM model in most of the study areas are less than −0.7. However, r values of the other two models in most areas of the four basins are higher than −0.5 (Figures 5a and 5b). Overall, the BS, BSS, and r values indicate that ASFP-ELM presents better performance for the 1- and 3-months lead times than those obtained by ASFP-RF and ASFP-SVR; it shows favorable skills for 1- and 3-months lead time ensemble and probability prediction in PRB, CRB, DRB, and ORB.

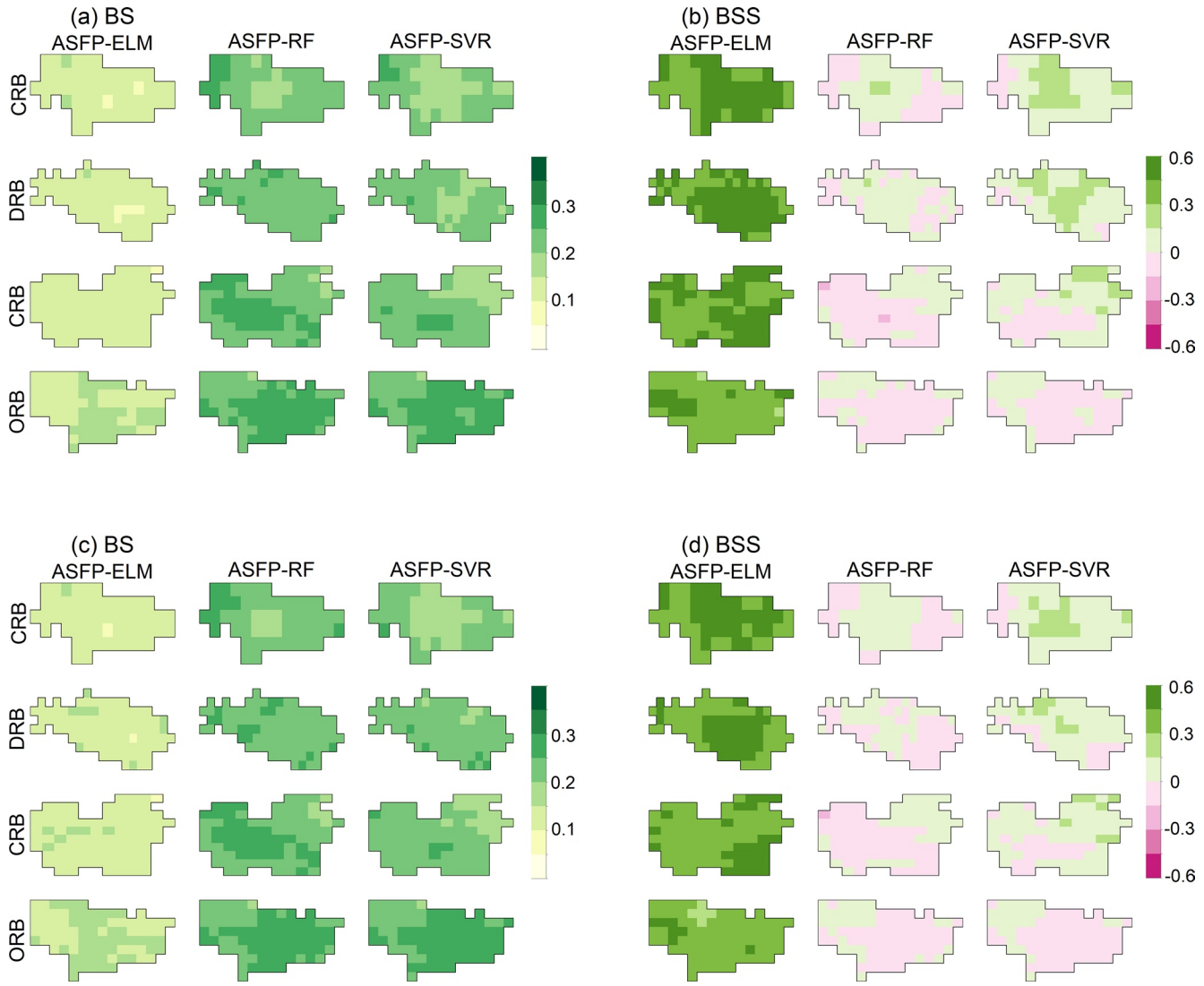

Figure 4. The BS and BSS metrics for probability prediction of the three models in four river basins. (a and b) 1-month lead prediction; (c and d) 3-months lead prediction.

4.2. Deterministic Prediction

Using the deterministic prediction outputs from 1989 to 2018, *r* values were initially applied to assessing the deterministic prediction (Figures 5c and 5d). The ASFP-ELM model fairly presents higher *r* values than ASFP-RF and ASFP-SVR models in these four basins. *r* values of the ASFP-ELM model in most of the study areas are larger than 0.7; this metric in almost the whole CRB and the eastern DRB even reaches to 0.8. However, *r* values of the other two models in most areas of the four basins are fairly less than 0.5. The *r* values of the 3-months lead time prediction share similar pattern with those of 1-month lead prediction. These imply that the ASFP-ELM model is fairly more skillful than the ASFP-RF and ASFP-SVR models for both 1- and 3-months lead time deterministic prediction.

Using nRMSE, AC, POD, FAR, BIS, and ETS, we further examine the model prediction performances (Figures 6, S7 and S8). The nRMSE values of the ASFP-ELM model are mostly between 10%–16% (Figure 6a), while the other two models present higher nRMSE values. In the ASFP-ELM model, the AC values are basically greater than 75% (Figure 6b), but low AC values (55%–70%) are found for the other two models. The POD values of the ASFP-ELM model are mostly greater than 70% (Figure 6c). In contrast, FAR values are mostly less than 25% (Figure 6d). The ASFP-RF and ASFP-SVR models show low POD values (<40%)

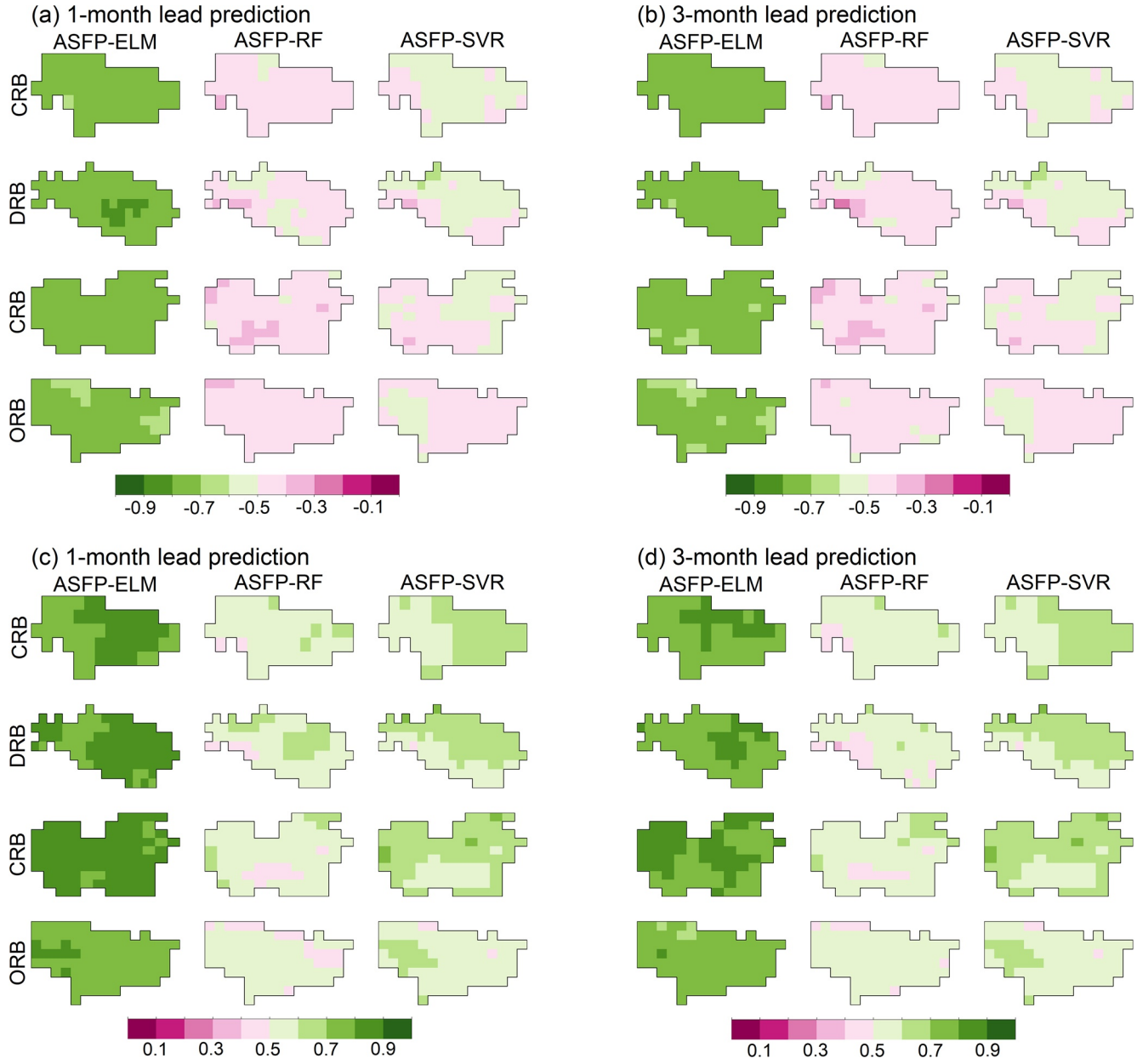

Figure 5. Correlation coefficients for probability (a and b) and deterministic (c and d) predictions of the three models in four river basins.

but relatively high FAR values (>25%). BIS values for the ASFP-ELM model are between 0.8 and 1.1 (Figure 6e), but this metric for ASFP-RF and ASFP-SVR models are generally smaller than 0.4. ETS values of the ASFP-ELM model are between 0.4 and 0.6 (Figure 6f), while ETS values for the other two models range from 0 to 0.2.

The spatial pattern of these several metrics for 3-months lead prediction is similar to that for 1-month lead prediction (Figures 7, S9 and S10). In the ASFP-ELM model, nRMSE values are mostly smaller than 16% (Figure 7a), while this metric for RF- and SVR-based models are between 16% and 22%. The AC values of the ASFP-ELM model are fairly higher than 75% (Figure 7b), while the other two models show low AC values (<70%). The ASFP-ELM model overall presents high POD values (>65%) but relatively low FAR values (<25%) (Figures 7c and 7d). POD values for the other two models are mostly smaller than 40%, but FAR values are higher than 25%. BIS values for the ASFP-ELM model indicate that the model, in general, does not tend to overestimate or underestimate droughts (Figure 7e), while the two models tend to underestimate

Figure 6. The six-evaluation metrics of the 1-month lead prediction obtained from the ASFP-ELM model in four river basins.

droughts. In the ASFP-ELM model, ETS values are in a range of 0.4–0.6 (Figure 7f), but are between 0 and 0.2 for the other two models.

4.3. Real-World Drought Events Prediction

The above evaluation metrics indicate the ASFP-ELM model outperforms ASFP-RF and ASFP-SVR models. To further test whether the ASFP-ELM model can fairly predict the spatiotemporal variations of droughts from both the deterministic and probabilistic aspects, several typical drought events across the four basins were chosen. Despite located in the humid climate zone, PRB suffered from exceptional drought during the autumn 2009 and the spring 2010 (Lin et al., 2015). As shown in Figures 8 and S11, the drought started to appear in west and east of the PRB in August 2009, with mild dry conditions, and then drought intensity gradually increased in the upper reaches in September; the prediction generally detects the drought onset. In October, drought became rather severe, and extended to the whole basin, which in accord with the model prediction; specifically, a good prediction for drought condition is found in the north region, with high probability of SPEI < -0.5, while it tends to underestimate the dry condition in the south region. Drought in the middle and lower reaches of the basin gradually faded away during the next few months; nevertheless, severe drought still persisted in the upstream areas during November 2009 and March 2010. The deterministic prediction overall reproduces the severe dry condition persisted in the west region, and the regions with a high probability of SPEI < -0.5 generally cover those with severe dry conditions revealed by observations. Drought intensity in these areas alleviated from April to May 2010, and deterministic and probability models both fairly predict such alleviation process, in accord with the previous study (Huang et al., 2021). Overall, the predictions well reflect this specific drought event over PRB.

A particularly extreme drought has hit Europe in 2003 (Rebetez et al., 2006). During February and March 2003, the drought was observed in the north of DRB, where a high probability of SPEI < -0.5 is detected

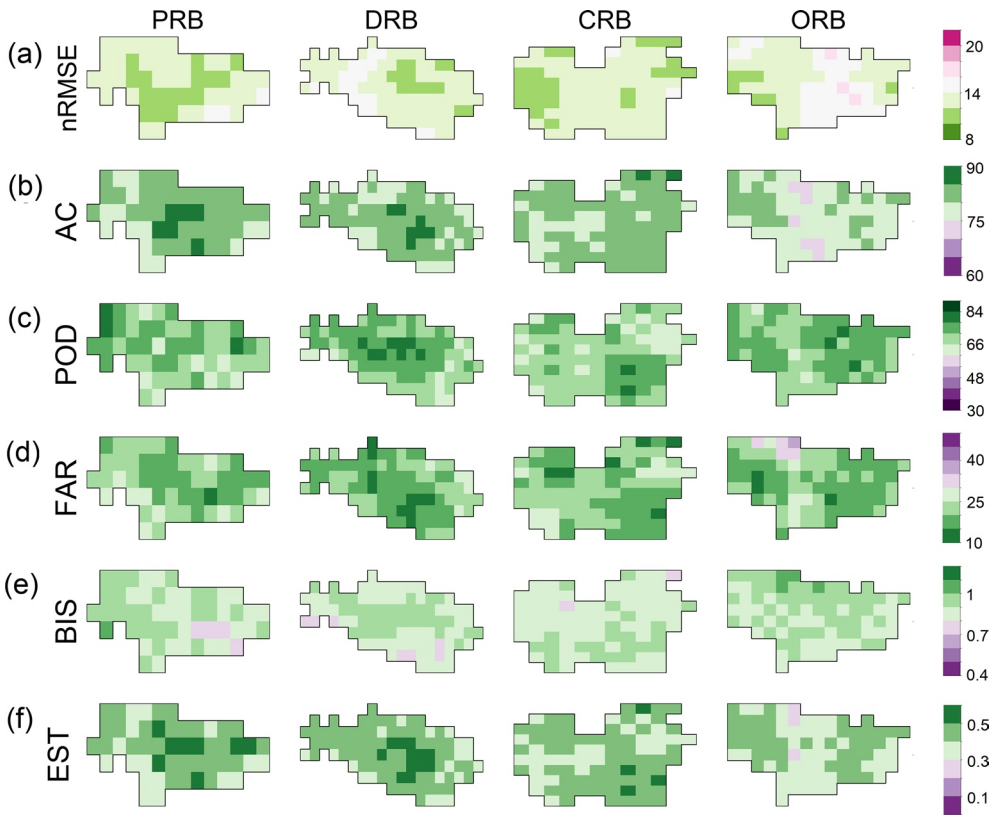

Figure 7. The six-evaluation metrics of the 3-months lead prediction obtained from the ASFP-ELM model in four river basins.

(Figures 9 and S12). It gradually spread throughout the basin in April and dry conditions became worse in May, as shown by prediction and observations; the drought probability largely increases across the whole region. The dry condition lasted for over 3 months in most of areas from June to August, as reported in Stojanovic et al. (2017); deterministic prediction fairly indicates this persistent dry condition, while it underestimates the dry condition in August, and the probability prediction presents a high probability of drought occurrence. Both prediction and observation indicate after that, drought intensity decreased and disappeared in most regions by November 2003, with low drought probability.

Drought in the west United States usually affects millions of people and causes widespread damages (He et al., 2017). Two typical drought events that respectively occurred in 1989 and 2017/2018 are selected for analyses in CRB. During March 1989, the drought began to occur in the south of CRB, with relatively large drought probability (Figures 10 and S13). However, both prediction and observation show that drought expanded to the whole basin and intensity became high in the next month. The severe dry condition persisted in the entire basin from May to June; the drought areas and category are fairly consistent with the observations, and the whole basin experienced high drought probability. Intensity gradually reduced from July to August, with decrease in dry probability. The other event started to appear in CRB during November 2017. Severe dry condition then extended to the whole basin in December and maintained until January 2018; probability prediction indicates the entire basin tends to suffer dry condition, as reflected by the deterministic model but with somewhat underestimation. It decreased during February but still stayed in most of the basin from March to April, which is generally predicted by both the deterministic and probability models. Prediction and observation show that drought again became severe in east part of the basin during May–June, when most regions experienced high drought probability. Though it still persisted in north of the basin with high probability, the intensity then gradually reduced in most of the areas during July–September. Such change is predicted by the deterministic model further indicating that the model has favorable skill. This event disappeared until October 2018, when most of the basin presents low dry probability.

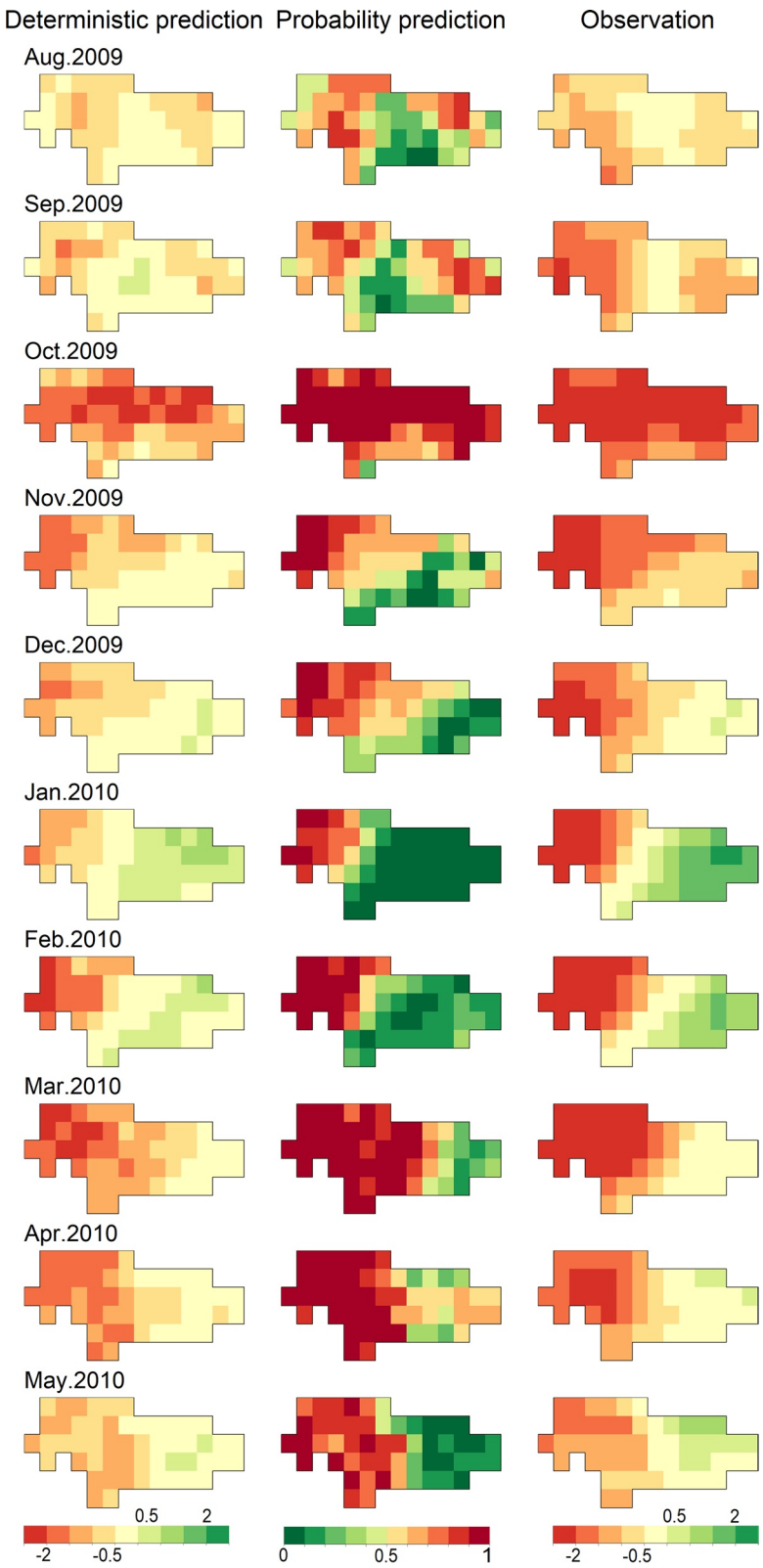

Figure 8. The spatial evolution of 2009–2010 drought based on observations and 1-month lead deterministic and probability (P (SPEI < −0.5)) predictions in the Pearl River basin.

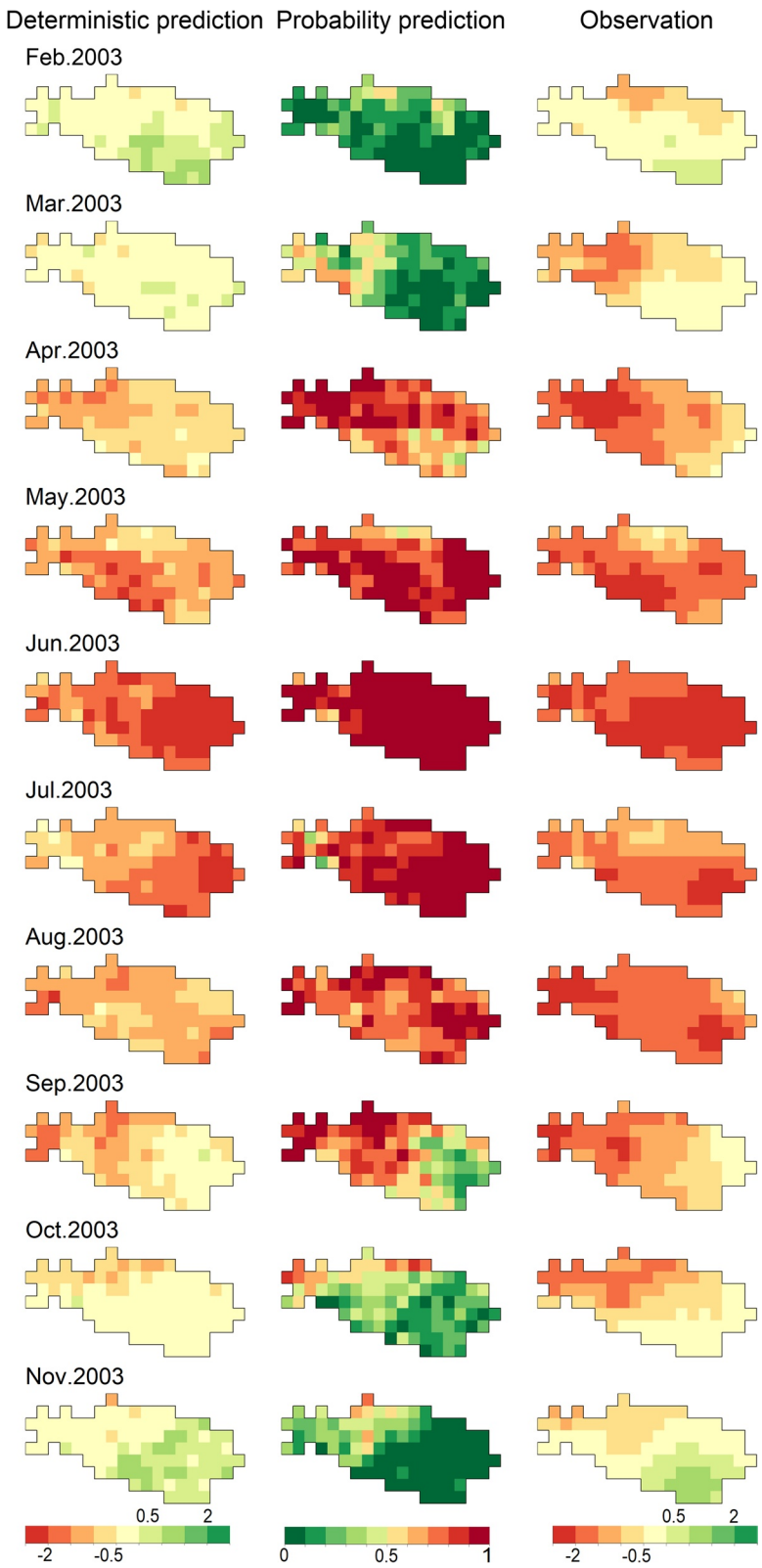

Figure 9. The spatial evolution of 2003 drought based on observations and 1-month lead deterministic and probability (P (SPEI < −0.5)) predictions in the Danube River basin.

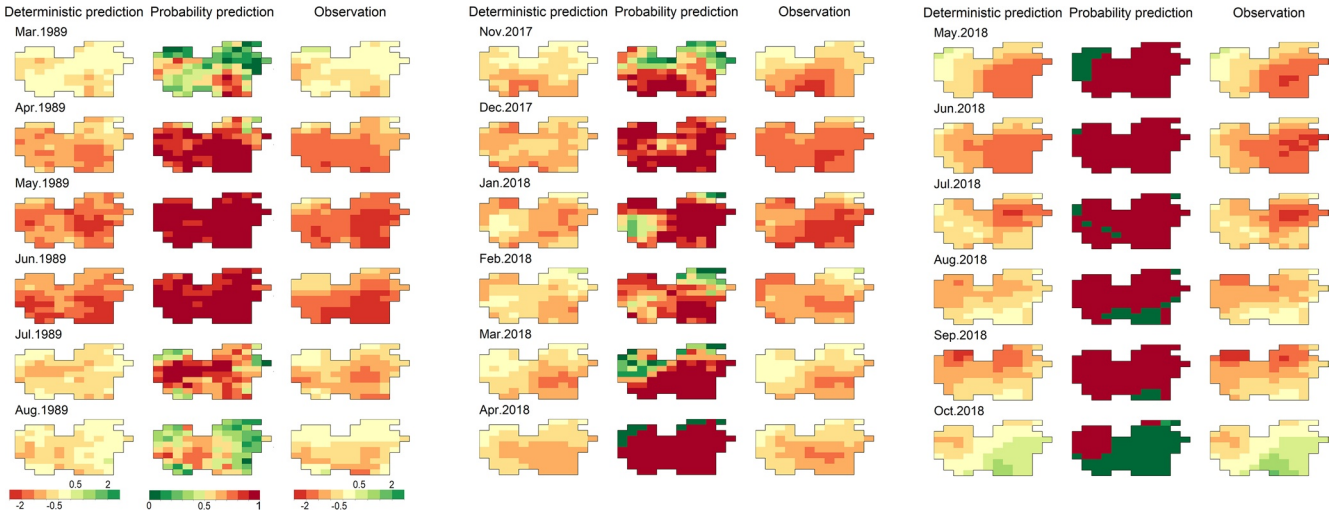

Figure 10. The spatial evolutions of droughts respectively occurred in 1989 and 2017–2018 based on observations and 1-month lead deterministic and probability (P (SPEI < −0.5)) predictions in the Colorado River basin.

Located in the southern African region, ORB is naturally prone to droughts (Masih et al., 2014). In 2015 and 2016, ORB experienced a severe drought triggered by warm sea surface temperature anomalies (Baudoin et al., 2017). The drought initiated in western basin in September 2015 as indicated by observations and predictions (Figures 11 and S14), while in the next month it propagated to the entire basin with increase of drought probability. In November, however, it became serious and severe dry condition persisted until December, while deterministic prediction shows less severe dry condition in December. Prediction and observation both show this event gradually faded away and disappeared in west of the basin during January–March in 2016, with decreasing drought probability. Mild dry condition was still scattered in the basin from April to June. However, this event again hit the western part of the basin in July 2016, and then spread to most areas in August and dry conditions lasted from September to December, which is well predicted by both the deterministic and probability models. The drought diminished during January 2017, when most of basin showed low drought probability. Overall, the drought patterns across the study regions indicated by 1- and 3-months lead predictions are fairly in accord with observations, indicating that the ASFP-ELM model can broadly predict the spatiotemporal variations in droughts under different climates.

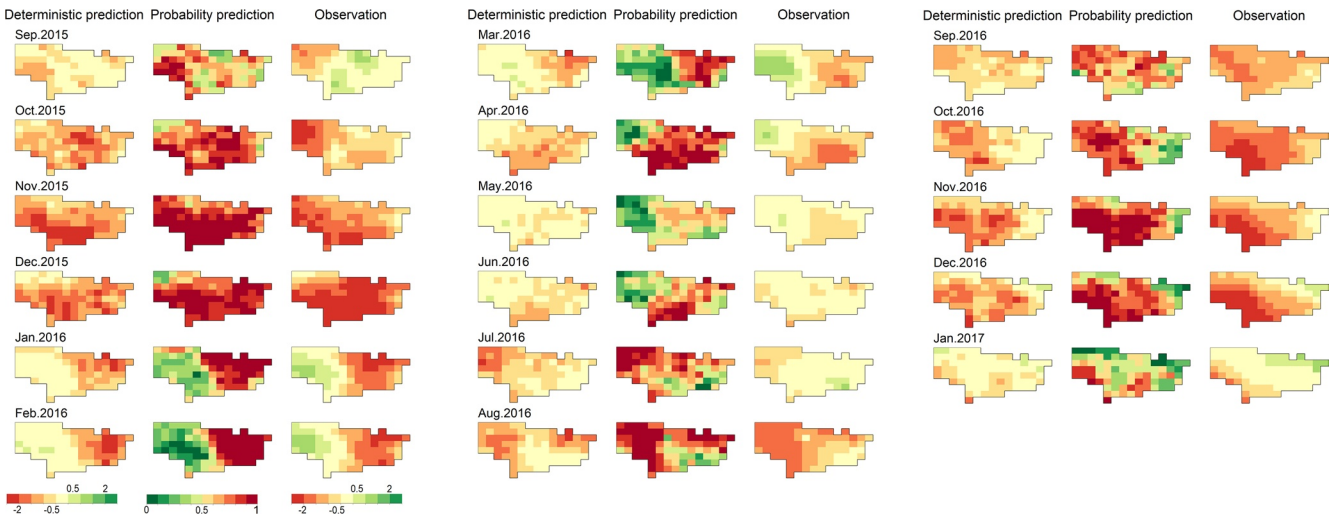

Figure 11. The spatial evolution of 2015–2016 drought based on observations and 1-month lead deterministic and probability (P (SPEI < −0.5)) predictions in the Orange River basin.

5. Discussion

5.1. Effectiveness of Different ASFPs in Drought Prediction

According to the definition of ASFP, the predictive ability of ASFP differs from one mode to another due to the different preceding SST signals. Taking the ASFP-ELM model as the example, we further show the different performances of these models using the nine ASFP patterns. For the 1-month lead prediction in PRB (Figure S15), when ASFP7 is employed, nRMSE and FAR values are lower and AC, ETS, and *r* values are higher than the remaining ASFP patterns, showing that ASFP7 is more predictive of droughts. In addition, ASFP1-based, ASFP5-based, and ASFP3-based models display relatively high satisfactory skills in DRB, CRB, and ORB, respectively. The assessment for the 3-months lead prediction is shown in Figure S16. The ASFP3-based model overall shows highest prediction in PRB, while ASFP1-based model presents best skill in DRB. For CRB and ORD, the best ASFP patterns are ASFP6 and ASFP5, respectively. These demonstrated that the way of combining SST signals in different time periods has an impact on the accuracy of drought prediction model, and that involving more SST information may not necessarily receive better prediction skill, for example, the 1-month lead prediction over PRB.

5.2. Decomposition and Grid Grouping Effects on Model Performances

Though the previous studies demonstrated that time series decomposition can improve model prediction (Belayneh et al., 2014), it is unclear whether the ASFP-based models coupling with STL-decomposition are indeed more accurate than without decomposition in terms of drought prediction. We further explore the prediction accuracy of the models without STL-decomposition. The parameterizations of the models without STL-decomposition are presented in Figures S17–S20, and the corresponding performances are shown in Figure S21. In combination with Figure 3, it can be found that the models with STL-decomposition outperform those without decomposition. A possible explanation is that the raw ASFP and SPEI series contain much noise reducing the prediction accuracy if no decomposition procedure is used (Belayneh et al., 2014).

In addition, this study does not merge any predictors between two neighboring oceanic grids. The identified ASFP over an oceanic grid is regarded as an independent predictor in the model. In some previous literatures, yet the identified neighboring oceanic grids are grouped (Chen & Georgakakos, 2014). Again, we test the model performances by grouping the identified neighboring oceanic grids (STL-decomposition considered). Figures S22–S26 respectively show the parameter specifications and model performances. Clearly, when grid grouping is used, the model performances have decreased accordingly. One possible reason for this is that machining learning methods usually require a variety of inputs for training. If neighboring grids are merged into one predictor, the inputs for ASFP-ELM, ASFP-SVR, and ASFP-RF would decrease substantially and the models cannot be trained sufficiently, leading to large biases in drought prediction.

5.3. Comparison With Other Approaches

Many studies have developed various drought prediction models for different regions, making important contributions to drought management. A comparison between the prediction models, including ours, is beneficial for the understanding of the differences between models and obtaining the most favorable one for practical drought prediction. However, partly due to the differences in the regions of interest and data availability, it is rather difficult to compare the performances of different models in detail. Su et al. (2021) shows that for the humid and semi-humid regions in China, including PRB, *r* values between simulated and observed drought characteristics during 1986–2005 are generally smaller than 0.3 according to the CMIP5 and CMIP6 models. Turco et al. (2017) used the European Centre for Medium-Range Weather Forecasts-System 4 to conduct prediction of summer droughts over Europe for 1981–2015. The correlations between observed and predicted SPEI across (not exactly) DRB largely range from 0.4 to 0.8. Using the multi-component satellite technique, Du et al. (2019) found that over the Southwestern United States, there is an overall moderate correlation (*r* values of 0.3–0.7) between surface wetness index and the Palmer moisture anomaly index in summer for the period of 2002–2017. Focusing on South Africa, Mehta et al. (2014) stated that the decadal correlations between actual and hindcast Self-calibrating PDSI are 0.2–0.6 overall. Compared to our findings, these possibly indicate that, to some extent, our approach introduced in the current study outperforms these traditional methods to varying degrees (Figure 5).

5.4. Caveats of the New Approach

The proposed approach in the current study provides useful and reliable tool for meteorological prediction. However, like other approaches at their first stages, it has some limitations. First, the water balance in SPEI is represented by the difference between precipitation and PET, and the use of PET in this index makes it somewhat difficult to interpret in water stressed situations, that is, when PET is far larger than actual evapotranspiration, which limits SPEI ability of monitoring droughts to some extent. In addition, the SPEI requires a wide range of data such as radiation, humidity and wind speed which are often more infrequently measured compared to precipitation. At the same time, this study employs the linear method to select predictors, which might loss the nonlinear signals between predictor and predictand. The nonlinear methods could be more appropriate for screening predictors as the inputs for machine learnings (Maier et al., 2010). Nevertheless, considering grid-based prediction is conducted with long records, STL-decomposition and time moving window method, the computational cost would increase distinctly if nonlinear techniques are used instead. In this regard, linear correlation is a favorable, though not the most appropriate method for the diagnosing useful SST signals.

Moreover, the new approach does not consider the commonly known SST variations such as ENSO, Pacific Decadal Oscillation and Atlantic Multidecadal Oscillation (Grantz et al., 2005), nor does it include any atmospheric circulation patterns as predictors. There are teleconnections across different oceanic zones (Dai, 2011); by extension, possible linkage between ASFP and other oceanic fluctuation patterns (e.g., ENSO) exist and needs further exploration, and the drought prediction models in the study may improve by combining the nine ASFP patterns with these oceanic fluctuation patterns. On the other hand, the circulation patterns due to variations in atmospheric pressure also play important role in drought onset and variations (Fu & Zeng, 2005; Manzano et al., 2019). For example, the North Atlantic Oscillation has shown to be one of the primary atmospheric circulations that impact the climate in Europe (Bonaccorso et al., 2015). Therefore, the performances of the models in this study could be further improved if circulation patterns related to atmospheric pressure are considered. More importantly, an exploration of the linkages between ASFP, the aforementioned known SST variations and circulation patterns could help reveal the physical mechanisms behind the screened ASFP and droughts across the regions of interest, which is conducive to the better understanding of SST impact on droughts.

6. Conclusions and Outlooks

In this study, we present a new meteorological drought prediction approach using ASFP and machine learning algorithms. The ASFP is constructed based on the antecedent SST fluctuations and serve as the drought predictors. Three models, that is, ASFP-SVM, ASFP-ELM, and ASFP-RF are constructed to produce ensemble, probability and deterministic predictions. To verify the models, four river basins including PRB, CRB, DRB and ORB across different continents are selected as the cases, where SPEI is predicted with 1 and 3 months lead times. Our findings demonstrate that the ensemble, probability, and deterministic predictions of ASFP-ELM outperform those of the other two models. Real-world drought predictions show that the spatiotemporal evolutions of historical severe droughts revealed by ASFP-ELM are fairly in accord with observations, which further demonstrates the applicability of the proposed drought prediction approach. In addition, there is little difference between the 1- and 3-months lead time predictions for all basins, indicating that ASFP-ELM has potential to yield robust seasonal prediction.

Covering ensemble, probability, and deterministic drought predictions, the new approach is deemed to provide more information for decision making. While the proposed approach provides an alternative, effective way for drought prediction in the case regions characterized by different climates and frequent droughts, it has potential to be applied in other regions, crucial for both social and environmental aspects such as integrated water resources management, drought risk mitigation, and ecosystem health issues. Given that drought is a complicated phenomenon with various influential factors, further studies should improve the proposed approach by combining other climatic factors such as ENSO and large-scale atmospheric circulation patterns.

Data Availability Statement

The precipitation and potential evapotranspiration datasets are publicly available from the Climatic Research Unit of the University of East Anglia (https://catalogue.ceda.ac.uk/uuid/10d3e3640f004c578403419aac167d82); the SST data set used are publicly available from the National Oceanic and Atmospheric Administration (https://psl.noaa.gov/data/gridded/data.cobe.html).

Acknowledgments
The research is financially supported by the Guangdong Basic and Applied Basic Research Foundation (2021A1515010935, 2019A1515111144), and the Water Resource Science and Technology Innovation Program of Guangdong Province (2020–2029). The authors thank the Editor and associate Editor, professor Ruping Mo as one reviewer, and the other anonymous reviewers for their thoughtful comments and suggestions that have greatly improved the manuscript.

References

AghaKouchak, A. (2014). A baseline probabilistic drought forecasting framework using standardized soil moisture index: Application to the 2012 United States drought. *Hydrology and Earth System Sciences*, *18*, 2485–2492. https://doi.org/10.5194/hess-18-2485-2014

Ali, M., Prasad, R., Xiang, Y., & Yaseen, Z. M. (2020). Complete ensemble empirical mode decomposition hybridized with random forest and kernel ridge regression model for monthly rainfall forecasts. *Journal of Hydrology*, *584*, 124647. https://doi.org/10.1016/j.jhydrol.2020.124647

Baudoin, M. A., Vogel, C., Nortje, K., & Naik, M. (2017). Living with drought in South Africa: Lessons learnt from the recent El Niño drought period. *International Journal of Disaster Risk Reduction*, *23*, 128–137. https://doi.org/10.1016/j.ijdrr.2017.05.005

Beguería, S., Vicente-Serrano, S. M., Reig, F., & Latorre, B. (2014). Standardized precipitation evapotranspiration index (SPEI) revisited: Parameter fitting, evapotranspiration models, tools, datasets and drought monitoring. *International Journal of Climatology*, *34*(10), 3001–3023. https://doi.org/10.1002/joc.3887

Belayneh, A., & Adamowski, J. (2012). Standard precipitation index drought forecasting using neural networks, wavelet neural networks, and support vector regression. *Applied Computational Intelligence and Soft Computing*, *2012*, 1–13. https://doi.org/10.1155/2012/794061

Belayneh, A., Adamowski, J., Khalil, B., & Ozga-Zielinski, B. (2014). Long-term SPI drought forecasting in the Awash River basin in Ethiopia using wavelet neural networks and wavelet support vector regression models. *Journal of Hydrology*, *508*, 418–429. https://doi.org/10.1016/j.jhydrol.2013.10.052

Bonaccorso, B., Cancelliere, A., & Rossi, G. (2015). Probabilistic forecasting of drought class transitions in Sicily (Italy) using standardized precipitation index and North Atlantic oscillation index. *Journal of Hydrology*, *526*, 136–150. https://doi.org/10.1016/j.jhydrol.2015.01.070

Breiman, L. (2001). Random forests. *Machine Learning*, *45*(1), 5–32. https://doi.org/10.1023/A:1010933404324

Chang, C. C., & Lin, C. J. (2011). LIBSVM: A library for support vector machines. *ACM Transactions on Intelligent Systems and Technology*, *2*(3), 1–27. https://doi.org/10.1145/1961189.1961199

Chen, C.-J., & Georgakakos, A. P. (2014). Hydro-climatic forecasting using sea surface temperatures : Methodology and application for the southeast US. *Climate Dynamaics*, *42*, 2955–2982. https://doi.org/10.1007/s00382-013-1908-4

Dai, A. (2011). Drought under global warming: A review. *Wiley Interdisciplinary Reviews: Climate Change*, *2*(1), 45–65. https://doi.org/10.1002/wcc.81

Deo, R. C., Kisi, O., & Singh, V. P. (2017). Drought forecasting in eastern Australia using multivariate adaptive regression spline, least square support vector machine and M5Tree model. *Atmospheric Research*, *184*, 149–175. https://doi.org/10.1016/j.atmosres.2016.10.004

Dikshit, A., Pradhan, B., & Alamri, A. M. (2020). Short-term spatio-temporal drought forecasting using random forests model at New South Wales, Australia. *Applied Sciences (Switzerland)*, *10*(12), 4254. https://doi.org/10.3390/app10124254

Diro, G. T., Grimes, D. I. F., & Black, E. (2011a). Teleconnections between Ethiopian summer rainfall and sea surface temperature: Part I-observation and modelling. *Climate Dynamics*, *37*(1), 103–119. https://doi.org/10.1007/s00382-010-0837-8

Diro, G. T., Grimes, D. I. F., & Black, E. (2011b). Teleconnections between Ethiopian summer rainfall and sea surface temperature: Part II. Seasonal forecasting. *Climate Dynamics*, *37*(1), 121–131. https://doi.org/10.1007/s00382-010-0896-x

Du, J., Kimball, J. S., Velicogna, I., Zhao, M., Jones, L. A., Watts, J. D., et al. (2019). Multicomponent satellite assessment of drought severity in the contiguous United States from 2002 to 2017 using AMSR-E and AMSR2. *Water Resources Research*, *55*(7), 5394–5412. https://doi.org/10.1029/2018wr024633

Feng, P., Wang, B., Luo, J., Liu, D. L., Waters, C., Ji, F., et al. (2020). Using large-scale climate drivers to forecast meteorological drought condition in growing season across the Australian Wheatbelt. *The Science of the Total Environment*, *724*, 138162. https://doi.org/10.1016/j.scitotenv.2020.138162

Frankignoul, C. (1985). Sea surface temperature anomalies, planetary waves, and air-sea feedback in the middle latitudes. *Reviews of Geophysics*, *23*, 357–390. https://doi.org/10.1029/RG023i004p00357

Fu, C., & Zeng, Z. (2005). Correlations between North Atlantic oscillation index in winter and eastern China flood/drought index in summer in the last 530 years. *Chinese Science Bulletin*, *50*(21), 2505–2516. https://doi.org/10.1007/bf03183642

Funk, C., Hoell, A., Shukla, S., Bladé, I., Liebmann, B., Roberts, J. B., et al. (2014). Predicting East African spring droughts using Pacific and Indian Ocean sea surface temperature indices. *Hydrology and Earth System Sciences*, *18*(12), 4965–4978. https://doi.org/10.5194/hess-18-4965-2014

Gobena, A. K., Weber, F. A., & Fleming, S. W. (2013). The role of large-scale climate modes in regional streamflow variability and implications for water supply forecasting: A case study of the Canadian Columbia river basin. *Atmosphere-Ocean*, *51*(4), 380–391. https://doi.org/10.1080/07055900.2012.759899

Grantz, K., Rajagopalan, B., Clark, M., & Zagona, E. (2005). A technique for incorporating large-scale climate information in basin-scale ensemble streamflow forecasts. *Water Resources Research*, *41*(10), W10410. https://doi.org/10.1029/2004wr003467

Hao, Z., & Singh, V. P. (2016). Review of dependence modeling in hydrology and water resources. *Progress in Physical Geography*. https://doi.org/10.1177/0309133316632460

Hao, Z., Singh, V. P., & Xia, Y. (2018). Seasonal drought prediction: Advances, challenges, and future prospects. *Reviews of Geophysics*, *56*(1), 108–141. https://doi.org/10.1002/2016RG000549

Harris, I., Jones, P. D., Osborn, T. J., & Lister, D. H. (2014). Updated high-resolution grids of monthly climatic observations—The CRU TS3.10 dataset. *International Journal of Climatology*, *34*, 623–642. https://doi.org/10.1002/joc.3711

Hateren, T. C. V., Sutanto, S. J., & Lanen, H. A. J. V. (2019). Evaluating skill and robustness of seasonal meteorological and hydrological drought forecasts at the catchment scale-case Catalonia (Spain). *Environment International*, *133*, 105206. https://doi.org/10.1016/j.envint.2019.105206

He, M., Russo, M., & Anderson, M. (2017). Hydroclimatic characteristics of the 2012–2015 California drought from an operational perspective. *Climate*, *5*, 1987–1992. https://doi.org/10.3390/cli5010005

Hsieh, W. W., Yuval, J., Shabbar, A., & Smith, S. (2003). Seasonal prediction with error estimation of Columbia river streamflow in British Columbia. *Journal of Water Resources Planning and Management*, *129*(2), 146–149. https://doi.org/10.1061/(asce)0733-9496(2003)129:2(146)

Huang, G. B., Zhu, Q. Y., & Siew, C. K. (2006). Extreme learning machine: Theory and applications. *Neurocomputing*, *70*(1–3), 489–501. https://doi.org/10.1016/j.neucom.2005.12.126

Huang, Z., Jiao, J. J., Luo, X., Pan, Y., & Jin, T. (2021). Drought and flood characterization and connection to climate variability in the pearl river basin in Southern China using long-term GRACE and reanalysis data. *Journal of Climate*, *34*, 2053–2078. https://doi.org/10.1175/jcli-d-20-0332.1

Ishii, M., Shouji, A., Sugimoto, S., & Matsumoto, T. (2005). Objective analyses of sea-surface temperature and marine meteorological variables for the 20th century using ICOADS and the Kobe collection, *25*, 865–879. *International Journal of Climatology*. https://doi.org/10.1002/joc.1169

Khan, M. S., & Coulibaly, P. (2006). Application of support vector machine in lake water level prediction. *Journal of Hydrologic Engineering*, *2*, 30–37. https://doi.org/10.1061/(asce)1084-0699(2006)11:3(199)

Kim, J. Y., Seo, K. H., Son, J. H., & Ha, K. J. (2017). Development of statistical prediction models for Changma precipitation: An ensemble approach. *Asia-Pacific Journal of Atmospheric Sciences*, *53*, 207–216. https://doi.org/10.1007/s13143-017-0027-2

Lee, S., Kim, J. C., Jung, H. S., Lee, M. J., & Lee, S. (2017). Spatial prediction of flood susceptibility using random-forest and boosted-tree models in Seoul metropolitan city, Korea. *Geomatics, Natural Hazards and Risk*, *8*, 1–19. https://doi.org/10.1080/19475705.2017.1308971

Li, B., & Cheng, C. (2014). Monthly discharge forecasting using wavelet neural networks with extreme learning machine. *Science China Technological Sciences*, *57*, 2441–2452. https://doi.org/10.1007/s11431-014-5712-0

Li, J., Wang, Z., Wu, X., Chen, J., Guo, S., & Zhang, Z. (2020). A new framework for tracking flash drought events in space and time. *Catena*, *194*, 104763. https://doi.org/10.1016/j.catena.2020.104763

Li, J., Wang, Z., Wu, X., Xu, C.-Y., Guo, S., & Chen, X. (2020). Toward monitoring short-term droughts using a novel daily scale, standardized antecedent precipitation evapotranspiration index. *Journal of Hydrometeorology*, *21*, 891–908. https://doi.org/10.1175/jhm-d-19-0298.1

Li, J., Wang, Z., Wu, X., Zscheischler, J., Guo, S., & Chen, X. (2021). A standardized index for assessing sub-monthly compound dry and hot conditions with application in China. *Hydrology and Earth System Sciences*, *25*, 1587–1601. https://doi.org/10.5194/hess-25-1587-2021

Lima, A. R., Cannon, A. J., & Hsieh, W. W. (2015). Nonlinear regression in environmental sciences using extreme learning machines: A comparative evaluation. *Environmental Modelling & Software*, *73*, 175–188. https://doi.org/10.1016/j.envsoft.2015.08.002

Lima, A. R., Cannon, A. J., & Hsieh, W. W. (2016). Forecasting daily streamflow using online sequential extreme learning machines. *Journal of Hydrology*, *537*, 431–443. https://doi.org/10.1016/j.jhydrol.2016.03.017

Lin, W., Wen, C., Wen, Z., & Gang, H. (2015). Drought in Southwest China: A review. *Atmospheric and Oceanic Science Letters*, *8*(6), 339–344. https://doi.org/10.3878/AOSL20150043

Liu, Z., Lu, G., He, H., Wu, Z., & He, J. (2018). A conceptual prediction model for seasonal drought processes using atmospheric and oceanic standardized anomalies : Application to regional drought processes in China. *Hydrology and Earth System Sciences*, *22*, 529–546. https://doi.org/10.5194/hess-22-529-2018

Loken, E. D., Clark, A. J., McGovern, A. M. Y., Flora, M., & Knopfmeier, K. (2019). Postprocessing next-day ensemble probabilistic precipitation forecasts using random forests. *Weather and Forecasting*, *34*(6), 2017–2044. https://doi.org/10.1175/WAF-D-19-0109.1

Ma, F., Ye, A., & Duan, Q. (2019). Seasonal drought ensemble predictions based on multiple climate models in the upper Han River basin, China. *Climate Dynamics*, *53*(12), 7447–7460. https://doi.org/10.1007/s00382-017-3577-1

Madadgar, S., AghaKouchak, A., Shukla, S., Wood, A. W., Cheng, L., Hsu, K. L., & Svoboda, M. (2016). A hybrid statistical-dynamical framework for meteorological drought prediction: Application to the southwestern United States. *Water Resources Research*, *52*, 5095–5110. https://doi.org/10.1002/2015WR018547

Maier, H. R., Jain, A., Dandy, G. C., & Sudheer, K. P. (2010). Methods used for the development of neural networks for the prediction of water resource variables in river systems: Current status and future directions. *Environmental Modelling & Software*, *25*(8), 891–909. https://doi.org/10.1016/j.envsoft.2010.02.003

Manzano, A., Clemente, M. A., Morata, A., Luna, M. Y., Beguería, S., Vicente-Serrano, S. M., & Martín, M. L. (2019). Analysis of the atmospheric circulation pattern effects over SPEI drought index in Spain. *Atmospheric Research*, *230*, 104630. https://doi.org/10.1016/j.atmosres.2019.104630

Masih, I., Maskey, S., Mussá, F. E. F., & Trambauer, P. (2014). A review of droughts on the African continent: A geospatial and long-term perspective. *Hydrology and Earth System Sciences*, *18*(9), 3635–3649. https://doi.org/10.5194/hess-18-3635-2014

Mehta, V. M., Wang, H., Mendoza, K., & Rosenberg, N. J. (2014). Predictability and prediction of decadal hydrologic cycles: A case study in Southern Africa. *Weather and Climate Extremes*, *3*, 47–53. https://doi.org/10.1016/j.wace.2014.04.002

Mishra, A. K., & Singh, V. P. (2012). Simulating hydrological drought properties at different spatial units in the United States based on Wavelet-Bayesian regression approach. *Earth Interactions*, *16*, 1–23. https://doi.org/10.1175/2012EI000453.1

Mo, K., & Lettenmaier, D. P. (2020). Prediction of flash droughts over the United States. *Journal of Hydrometeorology*, *21*, 1793–1810. https://doi.org/10.1175/JHM-D-19-0221.1

Muluye, G. Y. (2011). Deriving meteorological variables from numerical weather prediction model output: A nearest neighbor approach. *Water Resources Research*, *47*, W07509. https://doi.org/10.1029/2010wr009750

Niu, W., Feng, Z., Chen, Y., Zhang, H., & Cheng, C. (2020). Annual streamflow time series prediction using extreme learning machine based on gravitational search algorithm and variational mode decomposition. *Journal of Hydrologic Engineering*, *25*(5), 04020008. https://doi.org/10.1061/(asce)he.1943-5584.0001902

Park, S., Seo, E., Kang, D., Im, J., & Lee, M. I. (2018). Prediction of drought on pentad scale using remote sensing data and MJO index through random forest over East Asia. *Remote Sensing*, *10*(11), 1–18. https://doi.org/10.3390/rs10111811

Rasouli, K., Hsieh, W. W., & Cannon, A. J. (2012). Daily streamflow forecasting by machine learning methods with weather and climate inputs. *Journal of Hydrology*, *414–415*, 284–293. https://doi.org/10.1016/j.jhydrol.2011.10.039

Rebetez, M., Mayer, H., Dupont, O., Schindler, D., Gartner, K., Kropp, J. P., & Menzel, A. (2006). Heat and drought 2003 in Europe: A climate synthesis. *Annals of Forest Science*, *63*(6), 569–577. https://doi.org/10.1051/forest:2006043

Rhee, J., & Im, J. (2017). Meteorological drought forecasting for ungauged areas based on machine learning : Using long-range climate forecast and remote sensing data. *Agricultural and Forest Meteorology*, *237*(238), 105–122. https://doi.org/10.1016/j.agrformet.2017.02.011

Sadler, J. M., Goodall, J. L., Morsy, M. M., & Spencer, K. (2018). Modeling urban coastal flood severity from crowd-sourced flood reports using Poisson regression and random forest. *Journal of Hydrology*, *559*, 43–55. https://doi.org/10.1016/j.jhydrol.2018.01.044

Schubert, S. D., Stewart, R. E., Wang, H., Barlow, M., Berbery, E. H., Cai, W., et al. (2016). Global meteorological drought: A synthesis of current understanding with a focus on SST drivers of precipitation deficits. *Journal of Climate*, *29*(11), 3989–4019. https://doi.org/10.1175/JCLI-D-15-0452.1

Stojanovic, M., Drumond, A., Nieto, R., & Gimeno, L. (2017). Moisture transport anomalies over the Danube river basin during two drought events: A Lagrangian analysis. *Atmosphere*, *8*, 193. https://doi.org/10.3390/atmos8100193

Su, B., Huang, J., Mondal, S. K., Zhai, J., Wang, Y., Wen, S., et al. (2021). Insight from CMIP6 SSP-RCP scenarios for future drought characteristics in China. *Atmospheric Research*, *250*, 105375. https://doi.org/10.1016/j.atmosres.2020.105375

Sun, T., Zhang, T., Teng, Y., Chen, Z., & Fang, J. (2019). Monthly electricity consumption forecasting method based on X12 and STL decomposition model in an integrated energy system. *Mathematical Problems in Engineering*. https://doi.org/10.1155/2019/9012543

Sutanto, S. J., van Lanen, H. A. J., Wetterhall, F., & Llort, X. (2020). Potential of Pan-European seasonal hydrometeorological drought forecasts obtained from a multihazard early warning system. *Bulletin of the American Meteorological Society*, *101*, 368–393. https://doi.org/10.1175/BAMS-D-18-0196.1

Tian, M., Wang, P., & Khan, J. (2016). Drought forecasting with vegetation temperature condition index using ARIMA models in the Guanzhong Plain. *Remote Sensing*, *8*, 690. https://doi.org/10.3390/rs8090690

Turco, M., Ceglar, A., Prodhomme, C., Soret, A., Toreti, A., & Francisco, J. D.-R. (2017). Summer drought predictability over Europe: Empirical versus dynamical forecasts. *Environmental Research Letters*, *12*, 084006. https://doi.org/10.1088/1748-9326/aa7859

Verbesselt, J., Hyndman, R., Newnham, G., & Culvenor, D. (2010). Detecting trend and seasonal changes in satellite image time series. *Remote Sensing of Environment*, *114*, 106–115. https://doi.org/10.1016/j.rse.2009.08.014

Vicente-Serrano, Sergio, M., Beguería, S., & López-Moreno, J. I. (2010). A multiscalar drought index sensitive to global warming: The standardized precipitation evapotranspiration index. *Journal of Climate*, *23*, 1696–1718. https://doi.org/10.1175/2009JCLI2909.1

Wang, Ding, Y., Shao, Q., Xu, J., Jiao, X., Luo, Y., & Yu, Z. (2017). Bayesian multi-model projection of irrigation requirement and water use efficiency in three typical rice plantation region of China based on CMIP5. *Agricultural and Forest Meteorology*, *232*, 89–105. https://doi.org/10.1016/j.agrformet.2016.08.008

Williams, A. P., Cook, E. R., Smerdon, J. E., Cook, B. I., Abatzoglou, J. T., Bolles, K., et al. (2020). Large contribution from anthropogenic warming to an emerging North American megadrought. *Science*, *368*, 314–318. https://doi.org/10.1126/science.aaz9600

Xu, L., Chen, N., & Zhang, X. (2018). A comparison of large-scale climate signals and the North American Multi-Model Ensemble (NMME) for drought prediction in China. *Journal of Hydrology*, *557*, 378–390. https://doi.org/10.1016/j.jhydrol.2017.12.044

Zeng, Z., Hsieh, W. W., Shabbar, A., & Burrows, W. R. (2011). Seasonal prediction of winter extreme precipitation over Canada by support vector regression. *Hydrology and Earth System Sciences*, *15*(1), 65–74. https://doi.org/10.5194/hess-15-65-2011

Zhao, H., Gao, G., An, W., Zou, X., Li, H., & Hou, M. (2017). Timescale differences between SC-PDSI and SPEI for drought monitoring in China. *Physics and Chemistry of the Earth, Parts A/B/C*, *102*, 48–58. https://doi.org/10.1016/j.pce.2015.10.022